Exploring SDA Sensor Architectures for the Surveillance of Geosynchronous Spacecraft

James A. Blake[1,2], Don Pollacco[1,2], Robert Airey[1,2], Paul Chote[1,2], Benjamin F. Cooke[1,2], James McCormac[1,2], Billy Shrive[1,2], Richard West[1,2], Joshua Davis[3], Will Feline[3], Emma Kerr[3], Grant Privett[3], Yuki Akiyama[4], Hideaki Hinagawa[4], Shinichi Nakamura[4], Toshifumi Yanagisawa[4], Rebecca McFadden[5], Stuart Eves[6]

[1]*Centre for Space Domain Awareness, University of Warwick, UK*
[2]*Astronomy & Astrophysics Group, University of Warwick, UK*
[3]*Defence Science and Technology Laboratory, UK*
[4]*Japan Aerospace Exploration Agency, Japan*
[5]*Deimos Space UK Ltd*
[6]*SJE Space Ltd, UK*

ABSTRACT

Significant changes have taken place in the space domain over the past decade, with a growing number of emerging space-faring nations and commercial actors gaining access to the operational environment. The consequential diversification of space activities has brought about a need for a reassessment of space domain awareness (SDA) capabilities. Numerous states are developing their operational capability to undertake space-based activities, with potentially widespread ramifications for the safety of spacecraft. Rendezvous and proximity operations are becoming more prevalent in the geosynchronous (GSO) region for mission lifetime extension, active removal of debris, and satellite inspection, in all cases giving rise to novel challenges for SDA systems. What's more, there remains a largely uncharacterised population of small debris in the vicinity of the GSO region, uncovered by bespoke surveys with large aperture telescopes, and posing a significant risk to active satellites.

In 2022, the UK Space Agency commissioned a study into the requirements and opportunities for SDA in the UK, carried out by CGI with support from the Global Network On Sustainability In Space (GNOSIS) and UKspace. The study highlighted research and development of sovereign sensors as one of its key recommendations, both to improve the UK's sensing capability and to contribute to closing gaps in global SDA capability.

To this end, we explore the key requirements for future SDA sensor architectures, with a focus on ground-based electro-optical systems for the surveillance of spacecraft in the GSO region. Archival two-line element sets are used to simulate catalogued resident space objects (RSOs) passing through a grid of surveillance regions, tasked with monitoring the neighbourhoods of high-value assets in the vicinity of the geostationary belt, while the derived population from ESA's Meteoroid and Space Debris Terrestrial Environment Reference (MASTER) model is used as a basis for simulating the GSO debris field. We assess the observability of transiting RSOs from the vantage point of La Palma, Canary Islands, taking a variety of observational constraints into account, including the Earth's shadow, lunation, and the galactic plane.

We examine the performance of the simulated surveillance regions in the context of comprehensive, yet cost-effective SDA provision. Estimated costs are weighed against important metrics for essential SDA tasks (e.g., catalogue maintenance, change detection, and conjunction analysis), such as the total traffic observed per night, the cadence of the observations, and the temporal coverage of registered RSOs. The results of the simulation are used to inform a discussion of key sensor architecture requirements for effective SDA of GSO assets, taking into consideration a combination of sensor characteristics (e.g., sensitivity, resolution, and wavelength band) and other factors (e.g., geographical placement, site quality, and observational strategy) influencing SDA capabilities. We provide a commentary on the advantages and limitations of the different architectures considered and conclude with a list of recommendations for the designs of future SDA systems for the protection of GSO spacecraft.

1. INTRODUCTION

The protection of assets in the space domain is crucial to the uninterrupted provision of the space-based services that modern society relies upon. Over the past decade, the space operational landscape has evolved considerably, bringing about a need for a reassessment and enhancement of space domain awareness (SDA) capabilities. The rapid growth in the commercial space industry has given rise to a diversification of space activities, alongside a host of new challenges for the SDA community to overcome [1, 2].

The UK's National Space Strategy recognises the importance of establishing a safe and secure space domain, identifying SDA as one of four high-growth markets in which the UK seeks to develop global leadership [3]. In 2022, the UK Space Agency commissioned a study into the requirements and opportunities for SDA in the UK, produced by CGI with support from the Global Network On Sustainability In Space (GNOSIS) and UKspace [4, 5]. The study highlighted research and development for sovereign sensor improvements as one of its key recommendations, in order to boost the UK's sensing capability, contribute to closing gaps in global SDA capabilities, and strengthen existing international collaborations.

With these goals in mind, we explore the requirements for future SDA sensor architectures. Specifically, we focus on ground-based electro-optical systems for surveillance of the geosynchronous (GSO) region, where there is an increasing threat to space assets from dual-purpose rendezvous and proximity operations (RPO) [6, 7], and hazards posed by a largely uncharacterised population of faint debris [8–11] and an increase in crowding as operators make use of higher frequencies, enabling multiple spacecraft to operate in any given slot of the geostationary belt.

We take into consideration the following SDA challenges and tasks:

- *Catalogue maintenance*. With existing surveillance networks overstretched by a combination of unprecedented launch rates and an already substantial population of small debris, the attainable quality and quantity of tracking data for building/maintaining a catalogue and/or supplementing existing catalogues is a key consideration.
- *Object characterisation and classification*. The ability to go beyond mere detection, infer what a resident space object (RSO) is and how it is behaving, and diagnose strange or unexpected behaviour, is an essential goal for the next generation of SDA sensor architectures, in order to keep pace with the rapidly evolving operational landscape.
- *Early warning and attribution*. Timely and extensive coverage is also essential, to diagnose anomalies, monitor for change/manoeuvre detection taking place in the neighbourhood of key assets, and provide early warning of potentially nefarious activity.

To inform discussions throughout the paper, we define the following two modalities:

- *Survey*. Enhancing knowledge of traffic in the space domain, prioritising the detection, tracking, cataloguing, and characterisation of RSOs with completeness, efficiency, and precision.
- *Protect*. This mission instead concerns itself primarily with the protection of key assets, monitoring their surroundings for potentially nefarious activity, diagnosing anomalies, and providing rapid response to gather the necessary information for investigation in the event that something goes wrong.

In this paper, we present preliminary findings from a simulation of GSO traffic passing through surveillance regions of differing extent, centred on high-value spacecraft. We give an overview of the simulation framework in Section 2, outlining the propagation phase and the observational constraints accounted for, and identifying sources of uncertainty. Results from the traffic simulation are presented in Section 3 and used as the basis for a commentary on the advantages and limitations of different sensor architectures in relation to the two SDA missions listed above. We outline plans for future work in Section 4, before concluding with key recommendations for future GSO surveillance architectures.

2. TRAFFIC SIMULATION

To investigate the temporal performance of prospective SDA sensor architectures for monitoring GSO assets, we simulate traffic passing through a grid of surveillance regions, centred on particular targets of interest within the GSO

Table 1: Catalogue information for the Skynet and Astra satellite case studies. Sourced from Space-Track [12].

NORAD ID	Name	Source	Launch	Apogee [km]	Perigee [km]	Inclination [deg]	Period [mins]
29055	Astra 1KR	SES	2006-04-20	35802	35770	0.06	1436.07
32294	Skynet 5B	UK	2007-11-14	35802	35772	2.58	1436.12
33055	Skynet 5C	UK	2008-06-12	35807	35767	1.09	1436.11

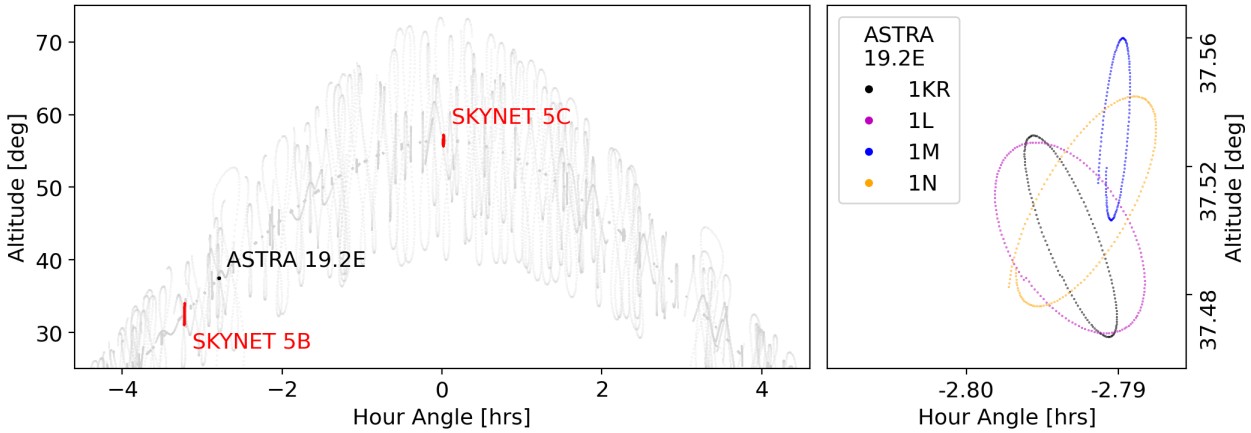

Fig. 1: Left) Orbital tracks in hour angle–altitude space for the Skynet (red) and Astra (black) satellites used as case studies, propagated for a duration of one sidereal day, on the night of 2023-02-22, from the vantage point of La Palma, Canary Islands. Tracks for other RSOs in the geosynchronous region are depicted by the grey background. Right) Zoomed-in view of the Astra 19.2° E constellation. Orbital state information sourced from Space-Track [12].

region. We consider two datasets as separate bases for the simulated GSO population:

- Archival catalogues (564 in total) of publicly available two-line element sets (TLEs), pulled daily from the Space-Track API [12] between March 2018 and August 2018, and subsequently between October 2018 and November 2019, in support of Warwick observing campaigns [13]. Specifically, the catalogues correspond to the 'Geosynchronous' sub-group, comprising objects which satisfy the following conditions: $0.99 \leq$ mean motion [revs/day] ≤ 1.01; and eccentricity < 0.01.
- A random realisation of the ESA Meteoroid and Space Debris Terrestrial Environment Reference (MASTER) 8 model [14] reference population, evolved to 2023. We opt to extract the 'Extended Geostationary Orbit (EGO)' population defined in [15], applying the following cuts: $37948 \leq$ semi-major axis [km] ≤ 46380; eccentricity ≤ 0.25; and inclination [deg] ≤ 25.

Hereafter, we refer to these populations as the 'archival' and 'MASTER' datasets, respectively.

The simulation is written in Python 3 and leverages a number of open source packages/tools, including `astropy` [16, 17], `matplotlib` [18], and `numpy` [19]. We also make use of the `tlemcee` [20] package, which builds from the `skyfield` [21] routines to manipulate and propagate TLEs, specifically those incorporating simplified deep space perturbation (SDP) models [22].

For each archival catalogue, we propagate the TLEs across the corresponding night, from the end of astronomical twilight in the evening, to the start of astronomical twilight in the morning, with a temporal resolution of 5 minutes. For the MASTER population, we generate acting TLEs from the Keplerian orbital elements for the extracted EGO population, taking sigma-clipped means from the archival TLE catalogues for the following parameters: ballistic coefficient [revs/day^2] $= -.00000113$; second derivative of mean motion [revs/day^3] 0; drag term [(Earth radii)$^{-1}$] 0. Note, however, that the former two choices are arbitrary in any case, as they are not used by the SGP4/SDP4 models employed by `skyfield`. The acting TLEs are propagated across a period of 60 days, centred on the reference epoch

for the random realisation of the MASTER population, in order to cover multiple lunar cycles. Each night is otherwise treated as outlined above for the archival dataset.

We identify several sources of uncertainty associated with the propagation phase of the simulation. Firstly, the accuracy of the TLEs themselves will be limited by a number of factors, such as the quality/quantity of observational data used to generate them, the fidelity of the force models used to propagate them, and a lack of *a priori* knowledge regarding active spacecraft manoeuvres taking place after their reference epochs [23]. For the archival dataset, all TLEs are propagated to within less than 24 hours of their reference epochs, while the aforementioned sources of uncertainty are likely to have a much more significant impact on the MASTER propagations, which stem from a single reference epoch. Furthermore, we treat the GSO region as a closed system during propagation, such that no objects are added to/removed from the region through launches, fragmentations, end-of-life missions, and so on. Of course, for the archival dataset, we account for these events on a nightly cadence (i.e., not in 'real-time'), as and when objects are added to/removed from the catalogue, though it is important to note that the catalogues themselves are far from complete, with the vast majority of GSO objects not bright enough to be detected/tracked by the Space Surveillance Network (SSN) with sufficient confidence to be catalogued. While anomalies and fragmentation events have significantly increased the population of GSO debris in recent years [10, 11], the Space-Track GSO sub-catalogue has only increased by roughly 200 objects, thus the archival dataset is largely representative of the present-day situation from a catalogued perspective.

At each timestep, the population of GSO objects visible from the vantage point of La Palma is inspected to register those traversing the simulated surveillance regions. We assess the observability of registered objects, taking into consideration the following four primary observational constraints:

- The object's altitude (elevation angle) must exceed an instrumental limit of 15°.
- The object must not be eclipsed by the Earth's shadow.
- Proximity to the galactic plane. Astrometric and object detection algorithms often struggle when presented with dense stellar fields, as the stars can significantly contaminate the images. Previous surveys of the GSO region [24] have found the level of image frames with significant stellar contamination to be less than 10% for galactic latitudes b exceeding $\pm 20^\circ$. For the simulation, we apply a less conservative constraint, flagging observations where $|b| < 15^\circ$ as a cause for concern, though a more rigorous treatment of this constraint will be considered for future development.
- Lunation. We draw from experience gained through previous Warwick survey operations [13], flagging observations that fail the following sequence of conditions as a cause for concern (i.e., those that are at significant risk of high background noise levels): lunar illumination < 0.95; projected object–Moon separation $> 130^\circ$ if illumination $\in [0.75, 0.95)$; separation $> 40^\circ$ if illumination $\in [0.50, 0.75)$; separation $> 20^\circ$ if illumination $\in [0.25, 0.50)$; and separation $> 10^\circ$ if illumination < 0.25.

The impact of adverse weather is currently not accounted for, though will be discussed further in Section 3.2 and considered in future work.

With size information available for the MASTER dataset, we are able to estimate object brightness as another factor influencing observability. In its simplified form, the visual magnitude m_V of an orbiting object may be expressed as [25, 26]

$$m_\mathrm{V} = m_\mathrm{sun} - 2.5 \log \left[\frac{\rho S}{R^2} f(\psi) \right], \tag{1}$$

where $m_\mathrm{sun} = -26.74$, ρ is the reflectivity, S is the cross-sectional (illuminated) area of the object and R is the distance between the object and the observer. We assume the objects to be Lambertian spheres with reflectivity $\rho = 0.1$, thus making use of the phase function for a diffuse sphere, $f(\psi) = \frac{2}{3\pi^2} [\sin \psi + (\pi - \psi) \cos \psi]$, where ψ is the solar phase angle, computed at each propagation timestep.

We consider three satellites as case studies for the traffic simulation, representing high-value assets at the centre of each surveillance region tested, with highest priority in terms of coverage: Skynet 5B, Skynet 5C, and Astra 1KR. All three satellites selected reside in the geostationary (GEO) belt, in recognition of the belt's importance to the provision of space-based services. Catalogued information for the satellites is provided in Table 1, while illustrative orbital tracks are shown in Figure 1, as viewed from the vantage point of La Palma.

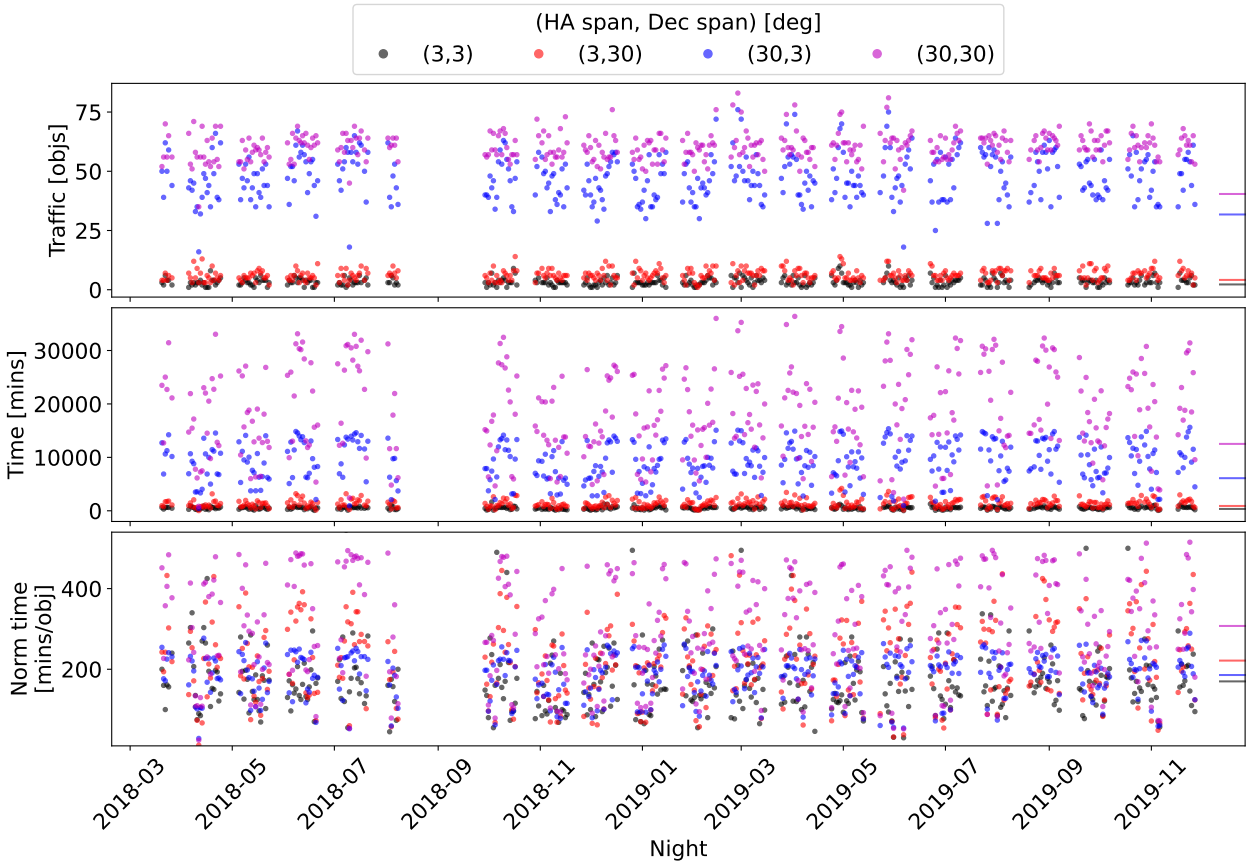

Fig. 2: Time series for archival traffic passing through the extremal surveillance regions centred on Skynet 5C: number of registered objects (top); total time for all registered objects (middle); and time per registered object (bottom). Only observations passing the four primary observational constraints listed in Section 2 are included. For clarity, nights with zero visible objects are excluded from the plot, but are accounted for in the overall means, marked for each region on the right-hand side. As mentioned previously, the nights corresponding to the large gap centred on 2018-09 are absent from the archival dataset.

3. RESULTS AND DISCUSSION

3.1 Simulated Traffic

The primary products from the simulation are related to nightly coverage, namely:

- Registered objects, observed within the region for at least two timestamps on the night in question, subject to a variety of observational constraints, as outlined in Section 2.
- Observation time accrued throughout the night for each registered object.

We also track catalogued information and angular rates for the registered objects, in addition to the on-sky separations between them and the central assets for the duration of the simulation.

In Figure 2, we show time series for archival traffic metrics extracted for the Skynet 5C case. We focus on the four extremal regions simulated, in terms of hour angle (HA) and declination (Dec) span, to investigate the influence of each on coverage. We find that large hour angle spans are typically the key to increasing traffic flow through the surveillance region. As the selected case studies reside in the GEO belt, a widening of the surveillance region in hour angle will bring more GEO satellites into view, while at the same time increasing the footprint of the 'fence' available to register objects on inclined orbits passing through the belt. That said, the traffic flow only gives an indication of the

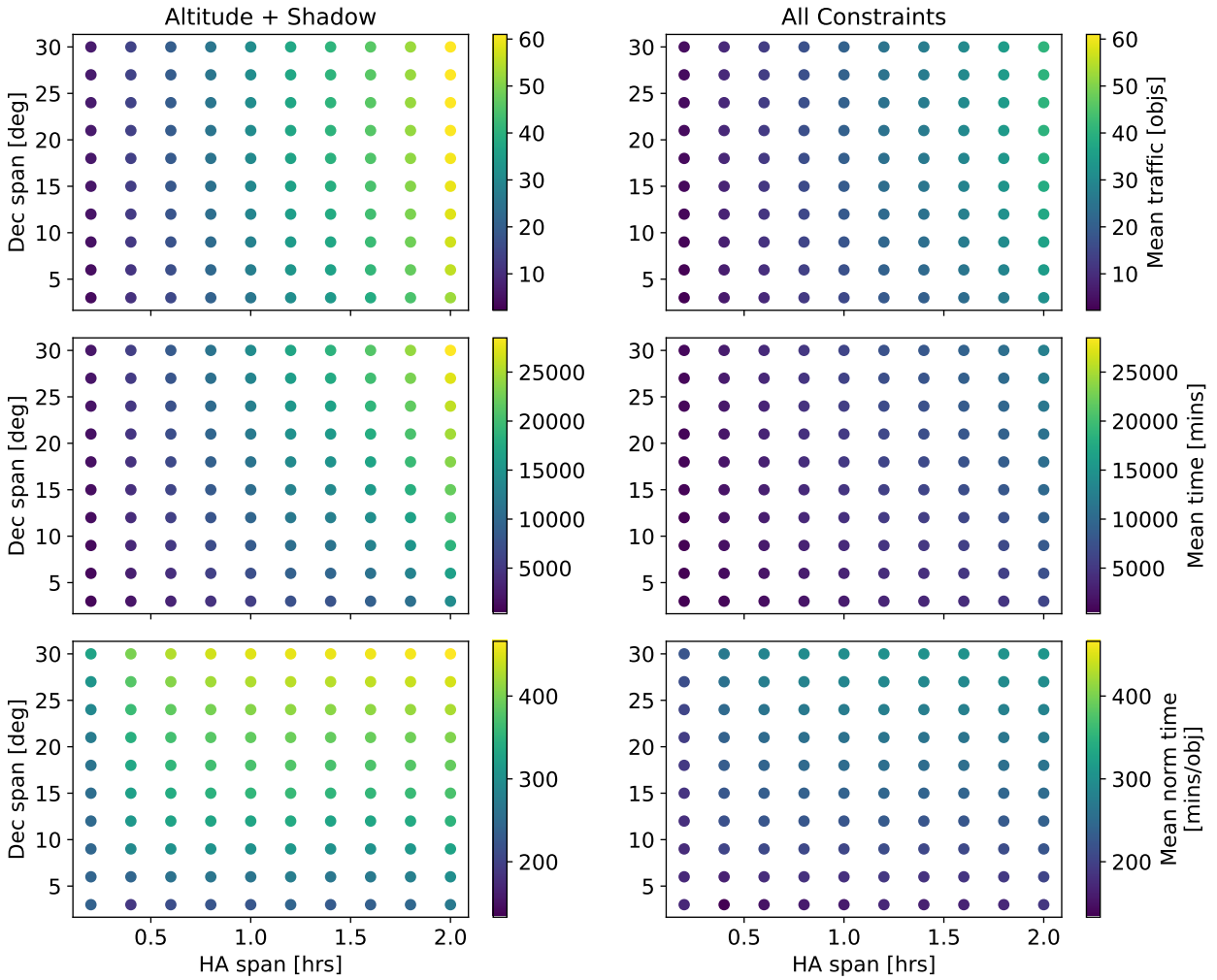

Fig. 3: Grids showing the mean number of registered objects (top), mean total time for all registered objects (middle) and mean time per registered object (bottom), across all available nights, for archival traffic passing through the surveillance regions centred on Skynet 5C. Traffic statistics are shown for observations passing the altitude and shadow constraints only (left) and for those passing all four primary observational constraints listed in Section 2 (right).

number of objects observed within the region over the course of the night. To gain an appreciation for the impact of region shape on the duration of observations per object, we consider the average temporal coverage for the registered RSOs in the bottom panel of Figure 2. We see significant variation in this metric from night to night, owing to its strong dependence on the observational constraints, many of which are themselves varying considerably in terms of impact throughout the year. Nevertheless, simulation-wide averages show that regions with larger declination spans tend to achieve higher temporal coverage per object. RSOs on inclined orbits passing through the GEO belt will have a predominantly north–south motion on-sky, thus calling for more extensive coverage along the declination axis.

These trends can be seen more clearly in Figure 3, where we consider averages of the coverage metrics, taken across all available nights comprising the simulation, for all surveillance regions tested. The severe impact of the lunar and galactic observational constraints is also clear, with the overall observation time per night reduced by more than half, as otherwise observable orbital arcs are cut short or vanish altogether due to unfavourable conditions. It is important to note, however, that we have treated all lunar and galactic flags as unobservable for the right-hand panels, and this should be considered a ‘worst case’ scenario. In reality, the observability will depend on a variety of other factors, related to the sensor characteristics and the intrinsic properties of the object, many of which will be discussed further in Section 3.2.

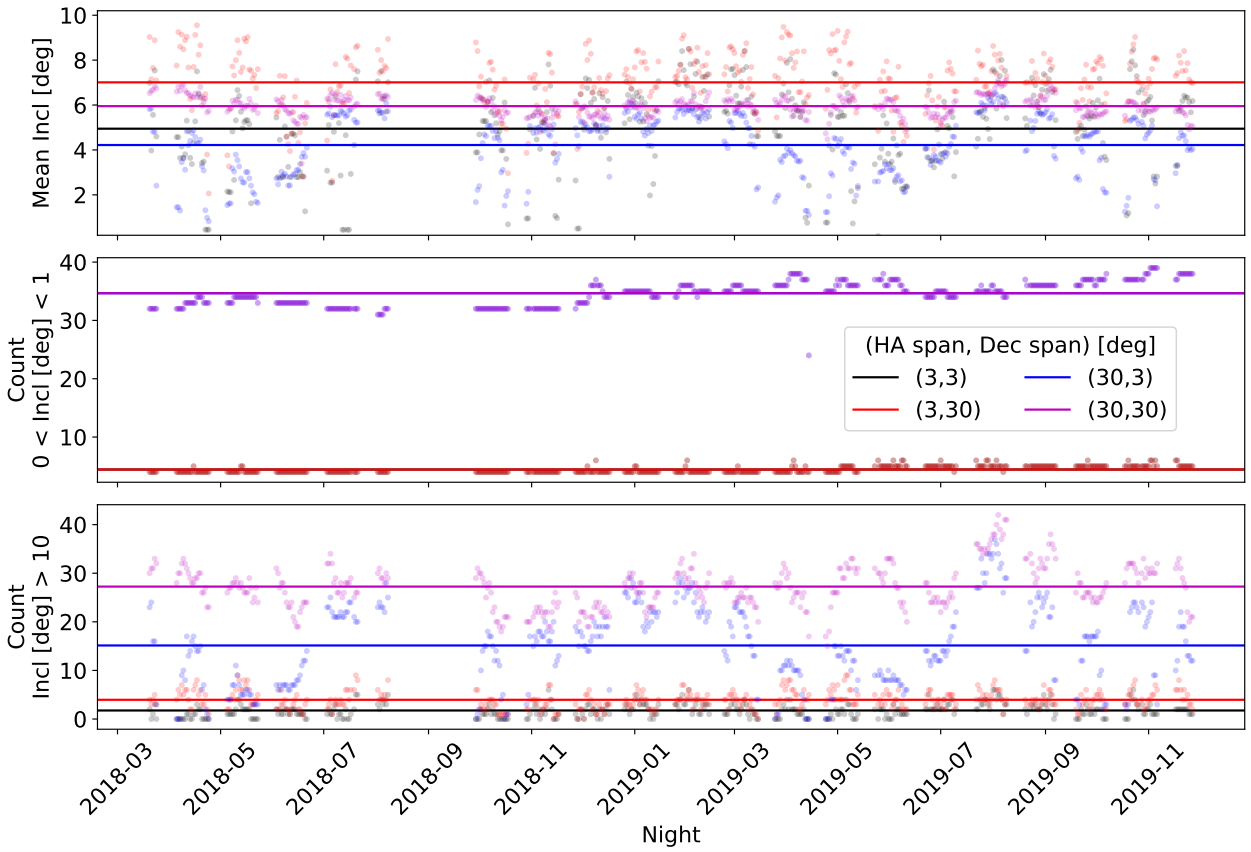

Fig. 4: Time series of inclination statistics for archival traffic passing through the extremal surveillance regions centred on Astra 1KR: mean inclination for registered objects (top); number of registered objects with an inclination between 0° and 1° (middle); and number of registered objects with an inclination exceeding 10° (bottom). Mean values across all nights overlay each plot. For the middle panel, note that the red markers overlay the black, while the purple markers overlay the blue, as the regions with equivalent hour angle spans share identical populations of low-inclination objects. Only observations passing the four primary observational constraints listed in Section 2 are included.

For the archival dataset, we are able to track the satcat information available from Space-Track for the registered objects. In Figure 4, we show time series of inclination statistics over the course of the simulation for Astra 1KR, focusing once again on the extremal surveillance regions. The simulation-wise average inclination is lower for large hour angle spans, as more GEO belt satellites are brought into view, with their near-zero inclinations. The gravitational interaction of the Earth with the Moon and the Sun induces a 53-year precessional cycle, whereby the inclination of a GEO satellite, if left unchecked, will oscillate from 0° to 15° and back to 0° again [27, 28]. Operational satellites in the GEO belt typically compensate for the effect of this perturbation with north-south station-keeping, ensuring their orbits remain as close to the equatorial plane as necessitated by their missions. The inclinations of uncontrolled objects (i.e., debris), on the other hand, will evolve accordingly.

This is a key distinction to account for when designing SDA sensor architectures for surveilling the GSO region, and its influence on the design will be strongly mission-dependent. For the *protect* mission defined in Section 1, for example, near-continuous monitoring of neighbouring operational satellites will be of paramount importance to ensure that potentially nefarious activity can be identified and monitored as early as possible. Systems conducting surveillance for *protect* purposes should therefore prioritise hour angle span, as supported by the middle panel of Figure 4, which shows the nightly number of near-equatorial objects registered by the extremal surveillance regions. Interestingly, a large hour angle span also tends to result in a higher registration rate for high-inclination objects, benefiting the *survey* mission by providing opportunities to detect and characterise debris. That said, the inclined objects will be passing through the region with a predominantly north-south motion, contrary to their GEO counterparts (which are near-

stationary in hour angle–declination space), and so a wider declination span would act to boost temporal coverage, helping to lengthen the orbital arcs available for initial orbit determination (for new/infrequent detections) and orbit refinement (for objects already catalogued).

3.2 Sensor architectures

In the following sections, we combine findings from the traffic simulation with a review of existing literature to provide a commentary on the advantages and limitations of different SDA sensor architectures, taking into consideration the *protect* and *survey* modalities defined in Section 1.

3.2.1 Observational cadence and strategy

The simulated surveillance regions are themselves near-fixed in hour angle and declination, owing to the geostationary nature of the central satellite's orbit and the pre-defined strategy used for the simulation. This ensures that photons of reflected light from the satellite (and other geostationary satellites within view) integrate over as few pixels as possible on the detector(s), thus maximising the signal-to-noise. Objects that are off-geostationary (e.g., GSO debris in inclined orbits) will exhibit some degree of angular motion relative to the field, with important implications for the observational strategies to be employed by the SDA system. For cases where the exposure time is greater than the time it takes for the object to traverse an angular pixel of the detector, a trailed morphology will manifest in the resulting image [see e.g., 8, 13], with a length governed by the relative angular rate of the object and a width set by the point spread function of the instrument. Targets of interest moving relative to the field in this way will often spend a mere fraction of a second contributing flux to any given source pixel on the detector. An exposure time longer than this will only serve to increase the noise contribution from the sky background, as the surface brightness spreads across an extended trail of pixels, rather than integrating over a localised group. By striking an accord between the exposure time and the expected pixel crossing time, an improved signal-to-noise can be achieved with a much higher observational cadence.

High-cadence observations are beneficial for a host of SDA tasks. In particular, the outputs of object characterisation and classification algorithms can be skewed by low temporal resolution, and high-cadence measurements act to fill gaps that would otherwise appear in the data [see e.g., 29]. Photometric light curves, for example, are an important tool for RSO characterisation, encoding information pertaining to the shape/size of the object, its surface properties and behaviour. Brightness variations can occur over a wide range of timescales, from sharp glints lasting for a fraction of a second, associated with small, highly-reflective components rapidly tumbling in and out of the observer's line of sight, to long-period features with characteristic timescales of hours to days, associated with stable periodic operations of active GEO spacecraft [9, 11, 13]. High-cadence imaging can help to resolve the intricate details of the former, reduce the level of blending with background stars, and more accurately map the attitudinal dynamics of the RSO [30]. For the *protect* mission, when paired with sophisticated algorithms, the monitoring of positional and brightness measurements in as close to 'real time' as possible could provide early warning of attitudinal/orbital manoeuvres, anomalies, and other changes of interest.

While short exposures are possible with traditional charge-coupled devices (CCDs), their long readout times lead to inefficient duty cycles, not suitable for the near-continuous imaging necessitated by rapidly varying SDA phenomena. Scientific Complementary Metal–Oxide–Semiconductor (sCMOS) devices show great promise for meeting this requirement, now available in large formats, with high quantum efficiencies and fast, low-noise readout electronics. The combination of short exposures and negligible readout overheads serves to enable high-cadence observations with the following advantages for SDA:

- The signal-to-noise of target RSOs is boosted, as trailing within the image is reduced.
- Trailing is also reduced for the background stars which, in the simulated configuration, will be moving through the surveillance regions at the sidereal rate. Shorter trails enable more accurate centroiding of sources within the image, improving the quality of the astrometric solution that feeds into orbital analysis.
- Shorter star trails give rise to lower levels of background contamination, reducing the frequency of source blending and increasing the searchable area to be targeted by object detection algorithms.

- The data rates of sCMOS cameras lend themselves well to the "blind stacking" technique, which can boost the detection limit by 1–2 magnitudes by stacking along paths of different direction and velocity within the image frame [31].

These benefits come at a price, however, both computationally and economically, owing to the enormous data rates associated with running large format imagers at such high cadences throughout the night. Efficient data management will be pivotal to the successful implementation of multi-node arrays routinely running sCMOS devices at sub-second cadence.

To inform discussions about observational strategy, we track the angular rates of objects registered by the surveillance regions over the course of the simulation. The along-track rates are computed using a rolling linear approximation between consecutive timestamps comprising the object's trajectory. We consider the angular rate as propagated, not as observed, and thus include all available timestamps, irrespective of observability. In the top panels of Figure 5, we investigate the links between mean angular rate and temporal coverage for the registered objects. By 'coverage', here, we refer to the fraction of available time in a given night where an RSO is observable, subject to all four primary observational constraints. A coverage of x % indicates that the corresponding RSO spent $(100-x)$ % of the available time unobserved, either due to poor observability or because the object's trajectory was not fully encompassed within the bounds of the surveillance region. To compare between nights of differing length, we take the equivalent of the shortest night sampled from the archival dataset to represent full (i.e., 100 %) coverage, before computing the mean and maximum coverage for different rate bins.

As expected, the temporal coverage tends to decrease with increasing angular rate, as lower-rate RSOs will typically remain within the surveillance region for longer and have a higher chance of avoiding areas of poor observability due to their smaller footprints on-sky. We find that superior coverages are attainable with larger declination spans for all rate bins, in agreement with the findings presented in Section 3.1, owing to the predominantly north-south motion of RSOs on inclined orbits passing through the GEO belt. A maximum coverage of 100 % is achieved by all extremal surveillance regions for the lowest rate bin, as this includes the central satellite itself (and any neighbouring geostationary satellites in view), which has a high chance of avoiding poor observability altogether on certain nights throughout the year with favourable galactic and lunar conditions. For large declination spans, the maximum coverage plateaus until the final rate bin, where the angular rate becomes too high for any RSO to achieve full coverage, while the surveillance regions with small declination spans exhibit a steep drop in maximum coverage, as off-GEO objects rapidly pass through the correspondingly narrow fences deployed.

We consider the typical orbital arc lengths observed for the different surveillance regions in the bottom left panels of Figure 5. The orbital arc length is an important consideration for both the *survey* and *protect* missions, each relying strongly on the quality of orbital information: the former to accurately catalogue objects transiting the region; and the latter to monitor changes and manoeuvres taking place in the vicinity of the central asset. Firstly, we focus on the priorities of the *survey* mission, specifically the goal of building and maintaining a catalogue of GSO objects. Due to the challenges associated with detecting debris in high-altitude orbits, surveys of the GSO region are often forced to invoke observational strategies/constraints to boost sensitivity and sky coverage, resulting in short orbital arcs for detected RSOs with long gaps between successive observations, rendering it impossible to compute a precise orbit from a single pass over the observation site [8, 24].

Numerous approaches have been developed to carry out data association for short orbital arcs [see e.g., 32–34]. We take inspiration from the authors of [35], who investigate the working boundaries of a novel technique to perform initial orbit determination using differential algebra, achieving success rates above 80 % in obtaining point solutions for raw GSO orbital arcs as short as 1–2 minutes, given sufficiently low uncertainties in the angles-only measurements (less than a few arcseconds). For the purposes of this study, we take a more conservative arc length of 10 minutes as the base objective for *survey* operations, requiring RSOs to register as observable for three or more timestamps, on account of the 5-minute temporal resolution of the simulation. With raw arcs of this length, the authors were able to analytically map the uncertainty region around the point solution and in many cases apply a least squares method to shrink the uncertainty.

For the *protect* mission, the primary goal will be to provide near-continuous coverage of the central asset and its neighbourhood. Breaks in coverage could mean that potential hazards and threats are missed, such as anomalies, fragmentation events, and close proximity manoeuvres, as observed for recent RPO missions [see e.g., 36]. We therefore set the base objective for *protect* operations to be the equivalent of the shortest night sampled from the

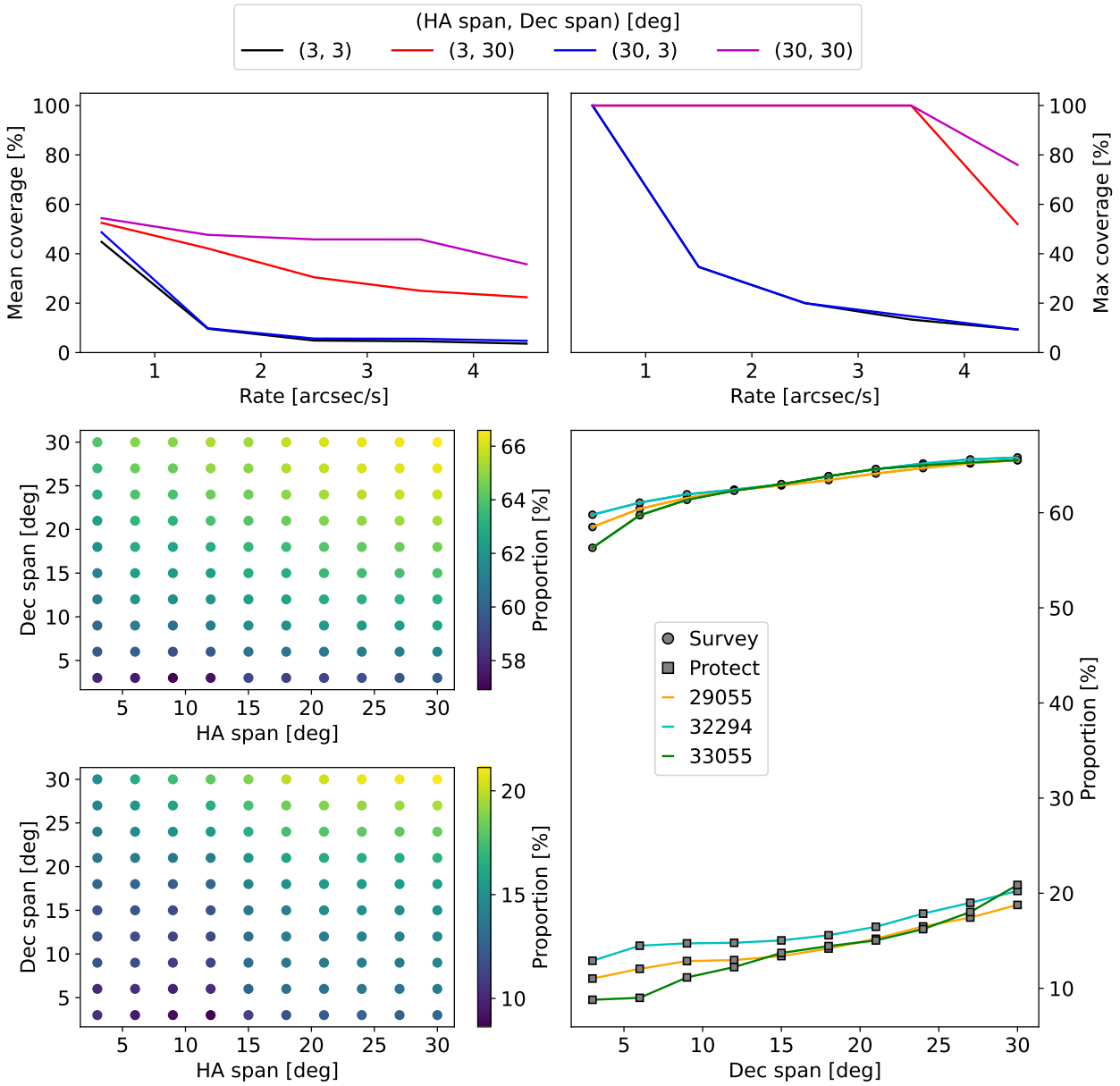

Fig. 5: Mean (top left) and maximum (top right) temporal coverage as a function of angular rate for archival traffic passing through the extremal surveillance regions centred on Astra 1KR. For the same case study, the proportion of orbital arcs satisfying a length of at least 10 minutes (*survey* objective in text, middle left) and the equivalent of the shortest night sampled from the archival dataset (*protect* objective in text, bottom left). For all case studies, the mean proportion of orbital arcs satisfying the *survey* and *protect* criteria, as a function of declination span, taken across all hour angle spans sampled (bottom right). In all panels, only observations passing the four primary observational constraints listed in Section 2 are included.

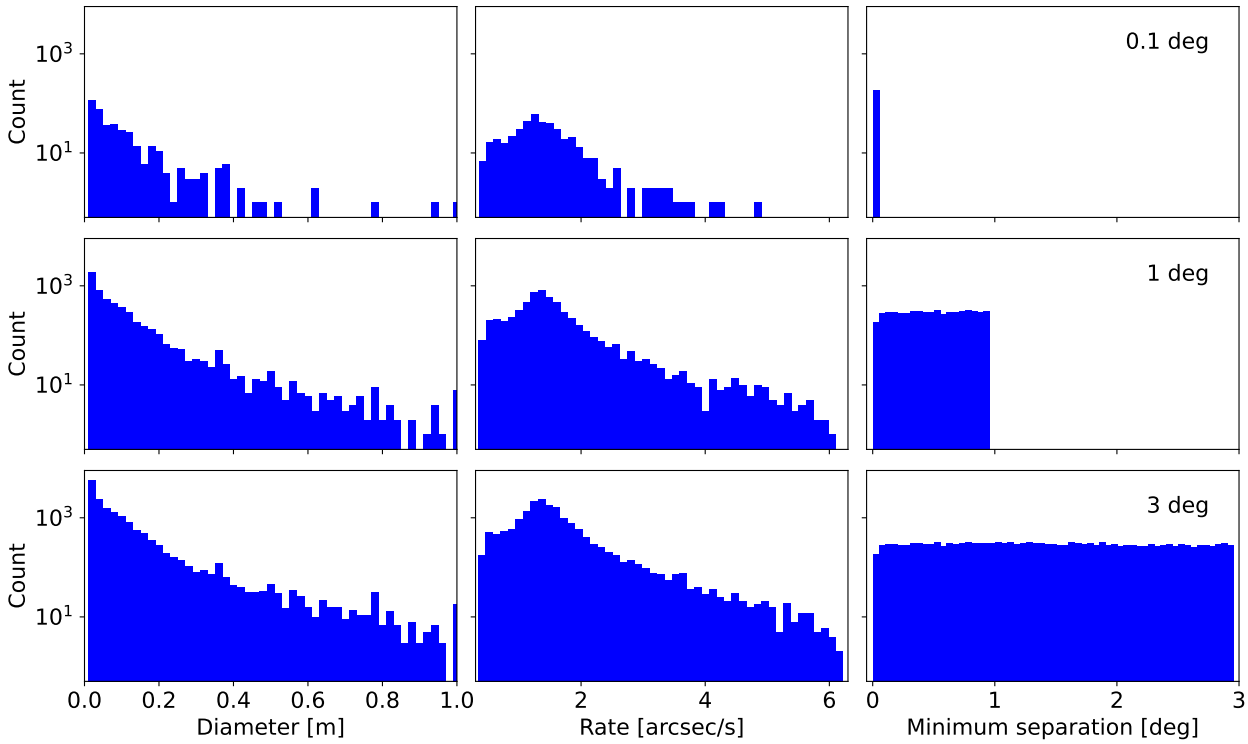

Fig. 6: Object size, angular rate, and minimum separation for MASTER traffic passing within 0.1° (top), 1° (middle), and 3° (bottom) of Astra 1KR over the course of the simulation. For illustrative purposes, all traffic is included, regardless of observability.

archival dataset, in order to compare nights of differing length. We find that roughly 56–67 % of orbital arcs observed for the Astra 1KR case satisfy the *survey* criterion, while roughly 9–21 % satisfy that of the *protect* mission. In both cases, the orbital arc length appears to benefit predominantly from an increase in declination span, in agreement with the previous discussions about coverage. We find similar (upward) trends for all case studies simulated, as shown in the bottom right panel of Figure 5, where we present the mean proportion of arcs satisfying the mission criteria, taken across all hour angle spans sampled. Flatter profiles are found when carrying out the same analysis for hour angle span.

3.2.2 Sensor characteristics

One of the most important sensor characteristics to consider for the SDA system is the sensitivity of the instrument(s) comprising it. The governing factor for sensitivity requirements will be the behaviour of fragmentation debris within the GSO region. Owing to the limitations of existing space surveillance networks, the (publicly available) archival dataset consists almost entirely of large satellites and rock bodies, with very few GSO fragmentation debris, despite considerable evidence pointing to the existence of a substantial population of small RSOs penetrating the region [see e.g., 8–11, 24, 37]. We therefore appeal to the MASTER dataset for the analyses that follow, which stems from a deterministic model of break-up events: those that are known/documented to have taken place in the past; and those that may have evaded detection, yet have been inferred through model validation with observational data [14, 38]. For the simulation, we use a subset of the overall population, extracted using the EGO cuts defined in Section 2. The cuts result in a base population of 15223 objects greater than or equal to 1 cm in size, compared to an average of roughly 1000 RSOs in the archival TLE catalogues.

When discussing specification requirements for the sensor(s) comprising the SDA system, it is essential to consider the properties of the RSOs to be monitored. In particular, object size is a key parameter influencing the brightness of targets to be observed. Surveys targeting the faint GSO debris population have used large-aperture (1 m-class

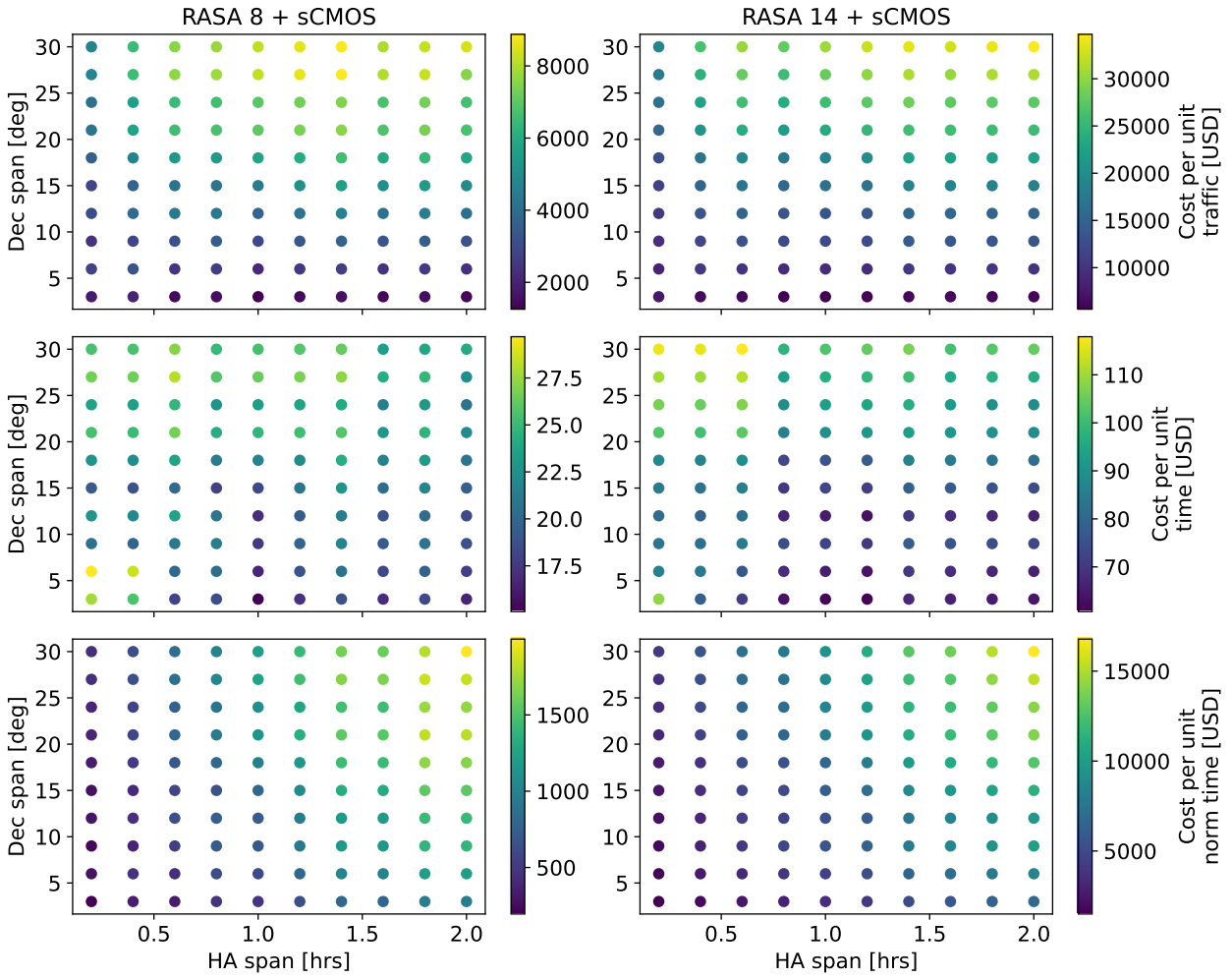

Fig. 7: Grids showing the mean estimated cost per unit traffic, time, and time per object, across all available nights, for MASTER traffic passing through the surveillance regions centred on Skynet 5C. Cost metrics are given for two possible array architectures: sCMOS detectors paired with 8-inch (left) and 14-inch (right) Rowe-Ackermann Schmidt astrographs. Only observations passing all four primary observational constraints listed in Section 2, in addition to the estimated sensitivity limits for the instruments, are included.

and above) telescopes to uncover objects around 10 cm in size (depending on the assumed shape and reflectivity, as in Equation 1), inferring the presence of even smaller RSOs from past fragmentation events [see e.g., 8, 24, 39]. Analyses of collision likelihood have found that relative velocities can reach as high as 4 $\mathrm{km\,s^{-1}}$ in the GSO region, suggesting that impactors as small as 20 cm could produce tertiary debris sufficiently large to spawn a collisional cascade [40]. Furthermore, with RPO activities becoming more frequent, CubeSat technologies are starting to proliferate in the GSO region, though examples to date are several 10 cm × 10 cm × 10 cm 'U' in size (e.g., Ascent [41]).

We track the on-sky separation of registered objects from the central asset as a by-product of the traffic simulation. In Figure 6, we show size and angular rate distributions for objects passing near to Astra 1KR over the course of the 60-day simulation for the MASTER dataset. Note that we include all traffic, regardless of observability, to get a complete sense of activity in the vicinity of the satellite. For the purposes of this study, we do not concern ourselves with the 3D separation distance, instead placing focus on the on-sky angular separation, which is more informative for discussions about sensor requirements. We find significant (and homogeneous) activity taking place within a projected radius of 3° surrounding the central asset. The vast majority of proximate traffic is small, mostly less than 50 cm in size and far below the nominal 1 m size cut-off of the SSN. Most of the RSOs have a relatively low on-sky angular rate between 0.5–2.5 $''\mathrm{s^{-1}}$, so could remain within the 0.1° boundary for several minutes.

The resolution requirements for the system will reflect the need to resolve GSO objects for as long as possible during close approaches (projected or otherwise), for instance during the pre-docking phases of RPO activities. Inspiration can be drawn from the Phantom Echoes 2 campaign, which tasked a variety of ground-based electro-optical sensors with monitoring the Mission Extension Vehicle-2 (MEV-2) RPO mission [6]. For expected RPO close approaches (e.g., those looking to service the central asset and/or extend its lifetime), the primary aim of ground-based surveillance is to monitor the approach phases before onboard sensors take over at a range of roughly 20–30 km (roughly 150″ angular separation) from the client spacecraft [42]. In the case of an unexpected approach (e.g., a conjunction with debris, or potentially nefarious activity), it will be important for the system to resolve the two objects for as long as possible, for the purposes of attribution and examination of intent. The 2 m Liverpool Telescope, with a (binned) resolution of $0.3''\text{px}^{-1}$, was able to spatially resolve MEV-2 and its client satellite when they were separated by less than 2 km, while small aperture, wide-field instruments lacked this capability. It should be noted that astronomical seeing due to atmospheric turbulence will ultimately prove the limiting factor for ground-based systems. Only the best astronomical sites (e.g., La Palma, Mauna Kea, etc) achieve sub-arcsecond median seeing for large parts of the year, while other potential sites would be limited to 1–5″ at best. While the system should provide warning of a close approach well in advance of such proximate encounters, high-resolution monitoring of the central asset's immediate neighbourhood will be important for enhancing awareness, maintaining accurate and precise positional information for tracking and conjunction analyses, and diagnosing the aftermaths of fragmentation events that may arise due to onboard malfunctions or collisions with small impactors.

For the MASTER dataset, we are able to apply additional observability cuts based on the brightness of registered RSOs, as described in Section 2. We use these cuts to explore the cost-effectiveness of two possible array-based solutions for tackling the missions discussed. For the purposes of this study, and in the context of comprehensive, yet cost-effective SDA provision, we place focus on commercial-off-the-shelf components that the authors have operational experience of. We opt for a QHY600M sCMOS detector for both architectures considered, allowing for high cadence observations as discussed in Section 3.2.1. The detector has a large 9576×6388 format, with a small 3.76 micron pixel size. Coupled with a high quantum efficiency, a low read noise, and a negligible readout time, and when combined with optics with short focal lengths, the QHY600M enables high-cadence, wide-field imaging with high resolution and high signal-to-noise. We pair the sCMOS detector with two Rowe-Ackermann-Schmidt astrographs (RASAs) of differing aperture sizes: 8-inch and 14-inch. As the light collecting area will be the primary factor governing the sensitivity of the instrument, this allows for a comparison between architectures with different mission goals in terms of detection limit. For the sub-second integration times required for high-cadence imaging, we estimate the detection limits of the 8-inch and 14-inch architectures to be $V \sim 16-18$ and $V \sim 17.5-19.5$, respectively, based on a consideration of instrument specifications (aperture size, focal length, filter bandwidth, pixel size, read noise, quantum efficiency) and the typical sky brightness for La Palma (and comparably dark astronomical sites), through different levels of lunation ($V \sim 19-21$ magnitudes per square arcsecond). From Equation 1, we find that these detection limits correspond to roughly $30-80$ cm and $15-40$ cm RSOs, respectively, for phase angles below 45°, assuming the objects to be Lambertian spheres with a reflectivity of 0.1, as in Section 2. These estimates place the performance of the RASA 8-inch configuration in line with the publicly-available data from the SSN, making it a promising candidate for the *protect* mission, capable of conducting high-cadence observations of neighbouring GEO belt satellites and monitoring the activity of large CubeSats and other spacecraft in the vicinity of the central asset. The estimated detection limits for the RASA 14-inch architecture, on the other hand, are comparable to those of surveys/operations involving much larger-aperture telescopes [see e.g., 24, 43], and of commercial SDA networks targeting the GSO region. This aligns well with the goals of the *survey* mission, enabling the detection of (faint) uncatalogued, yet hazardous debris in favourable lunar conditions, and the monitoring and orbit refinement of (bright) catalogued objects, even in poor lunar conditions. It is worth noting that the detection limits of both architectures could be further improved by optimising the observational strategy for blind stacking [31], as discussed in Section 3.2.1.

We take ballpark cost estimates for the above components and compute the cost per unit traffic, time, and time per object for registered traffic passing the four primary observational constraints and an appropriate detection limit for the architecture in question. For the purposes of this study, we set representative limits of $V = 17$ and $V = 19$ for the RASA 8-inch and 14-inch configurations, respectively. We also reserve discussion of other costs (e.g., computing, enclosure, mount) for a future study, as these will vary significantly depending on the number of nodes comprising the array and the strategy employed. The results for the Skynet 5C case are shown in Figure 7. We find that the RASA 8-inch arrays are generally the more cost-effective option if: (i) objectives align with the *protect* mission; and (ii) budget restrictions are the primary concern. However, it is important to keep in mind that the registered traffic will

be significantly boosted by the larger aperture and fainter detection limit of the RASA 14-inch configuration. For the *survey* mission, this would certainly justify the higher cost, as uncovering faint and uncatalogued debris will be of paramount importance to mission success. That said, the boosted traffic may also justify a higher cost for the *protect* mission, as an increased awareness of the hazard posed by small (faint) debris in the vicinity of the central asset will enhance the system's diagnostic and protective capabilities.

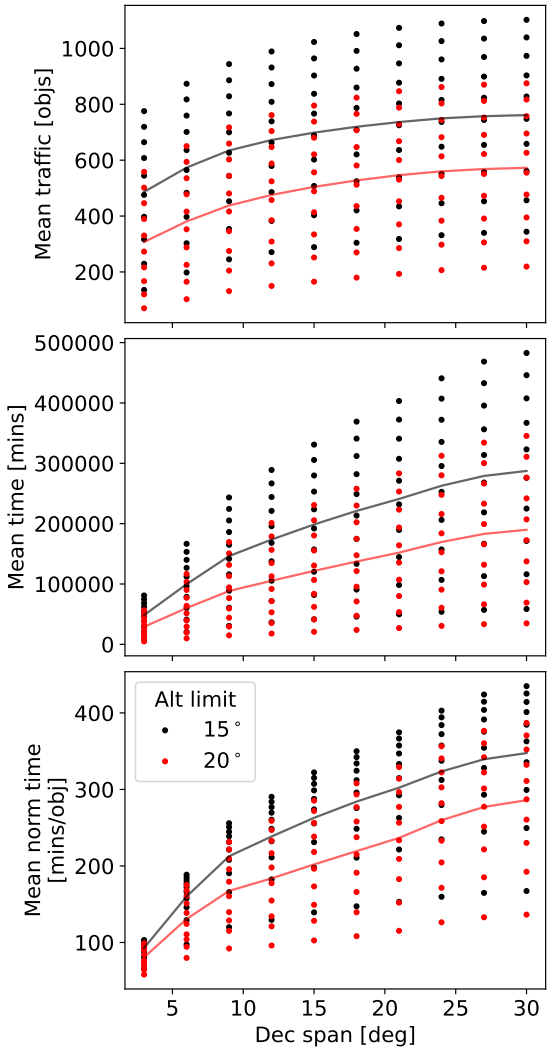

Fig. 8: Mean traffic (top), mean time (middle), and mean time per object (bottom) for MASTER traffic passing through the surveillance regions centred on Skynet 5B. Traffic metrics for all regions are plotted as a function of declination span, with averages over all hour angle spans indicated by the solid lines. A significant reduction in all metrics is observed for the higher instrumental altitude limit (red), owing to the central satellite's low altitude.

For each architecture, we notice similar (and familiar) trends across the surveillance regions simulated. In Section 3.1, we found that increasing the width of the observational fence along the GEO belt is the most effective way of boosting registered traffic, as it increases the chance of catching RSOs in inclined orbits passing through the belt, while also bringing into view neighbouring GEO satellites. It therefore comes as no surprise that, in terms of traffic registration, the most cost-effective architectures are those with small declination spans, as additional layers along the declination axis will have little impact on the number of objects registered, but a significant impact on the overall cost of the facility. Conversely, when considering the time per registered object, we find that the most cost-effective arrays are those with small hour angle spans, as additional layers along the hour angle axis will have a limited effect on the coverage of inclined RSOs with their predominantly north-south motion, though the trend is less stark than that for the traffic above. A compromise that appears to suit both sets of mission priorities while keeping costs comparatively low would be a surveillance region with an hour angle span in the range $0.8 - 1.2$ hrs, and a declination span between 9° and 15°.

3.2.3 Combatting observational constraints

For ground-based optical components of an SDA system, there will inevitably be gaps in coverage due to daylight, weather, and maintenance. For the *protect* mission in particular, it will be important for the system (through a combination of instrumentation, observational strategy, and software) to be able to identify changes and events that take place during these periods of deadtime. Methods of reducing this deadtime include the incorporation of infrared and/or passive radio frequency (RF) sensing to extend the window of observation into the daytime and/or periods of poor weather conditions [44], or the re-tasking of quiet nodes of the array, in order to ensure multiple layers of contingency for essential tasks. The former would also boost the system's capability to assess the status of RSOs; RF signals indicate active transmissions, while infrared measurements (across multiple bands) can highlight the presence of active onboard sub-systems and probe the material composition of the spacecraft's surface [45]. Deploying a multi-site network of sensors is a tactic that is commonly employed by commercial SDA operators, with their optical sensor networks often exploiting wide geographical distributions, in order to ameliorate local weather interruptions and close the daytime gap for more extensive coverage of targets in the GSO region [11]. Space-based sensors can overcome many of the limitations associated with ground-based optical surveillance, bypassing atmo-

spheric interference and avoiding weather/daytime outages, however space-based SDA solutions remain costly and come with their own challenges related to sensor management and maintenance [46, 47].

Event-based sensing is another technique that could contribute to reducing the daytime gap. Unlike their frame-based counterparts (e.g., CCD and sCMOS), which output image frames of pixel intensities, neuromorphic cameras produce a continuous stream of events, generated when pixels detect a change in log light intensity [48, 49]. Neuromorphic sensors have pixels that operate asynchronously and independently, rapidly responding to changes in brightness in the scene as they happen, and otherwise remaining silent. This enables the acquisition of event-based data with high temporal resolution, while greatly reducing the amount of redundant information being captured, thus keeping data rates much lower than those associated with sCMOS cameras running fast, for example. Furthermore, with a high dynamic range and an ability to detect small changes in brightness across a wide range of background intensities, neuromorphic cameras show great promise for tackling some of the common observational constraints that often blight optical GSO surveillance systems.

4. FUTURE WORK

The simulated surveillance regions for this study have been centred on selected assets, primarily to investigate the behaviour of GSO traffic in their vicinity. Of course, this may not represent the most cost-effective or efficient observational strategy when considering a particular asset or mission. Depending on budgetary constraints, it may prove beneficial to employ a scanning strategy, whereby one or more array nodes are used to scan a surveillance region larger than their combined field of view, at a cadence that can be tuned to suit the needs of the mission in question. This would lead to a reduction in temporal coverage, strongly impacting the goals of the *protect* mission, but may prove sufficient to meet the needs for the *survey* modality. The efficiency of the SDA architecture could also be significantly boosted by re-tasking redundant nodes, for example those unable to observe RSOs due to one or more observational constraints. To highlight the importance of node re-tasking, we investigate the impact of raising the instrumental altitude limit for the low-altitude Skynet 5B case study. In Figure 8, we show the regional traffic metrics for altitude limits of 15° and 20°. The higher altitude limit has a negative effect on all traffic metrics, shortening orbital arcs or missing them altogether, and several nodes would need to be re-tasked to image elsewhere to avoid redundancy.

We aim to conduct a follow-up study to build upon the preliminary findings presented here by carrying out the following investigations:

- Supplementing the basis population for the simulation with other orbital regimes of interest, such as geostationary transfer and highly eccentric orbits, where recent fragmentation events have generated hundreds of debris on orbits that penetrate the GSO region.
- Considering alternative observational strategies to boost cost effectiveness and exploring their implications for the different SDA modalities.
- Considering a wider variety of sensors and techniques as candidate architectures, for example larger-aperture telescopes, and the incorporation of infrared and/or neuromorphic sensing.
- Considering a multi-site network and its implications for SDA performance. This will build on our collaboration between the University of Warwick, the Defence Science and Technology Laboratory (UK), and the Japan Aerospace Exploration Agency.

5. SUMMARY

We have carried out a simulation of surveillance regions of differing shape and extent, centred on high-value assets in the geosynchronous region, in order to investigate the behaviour of nearby traffic and explore potential implications for future SDA sensor architecture requirements. Throughout the paper, we have interpreted results in the context of two key SDA modalities: (i) *survey*, with a primary aim of detecting, cataloguing, and characterising objects; and (ii) *protect*, where monitoring for changes and potentially nefarious activity in an asset's neighbourhood is the highest priority. For the base population of the simulation, we have drawn from two separate datasets: (i) archival two-line element catalogues from Space-Track; and (ii) the European Space Agency's MASTER 8 model reference population,

evolved to 2023. The available orbital state information was propagated to explore the temporal evolution of traffic passing through the simulated surveillance regions, accounting for a range of observational constraints, such as the Earth's shadow, lunation, and the galactic plane.

We have combined an examination of traffic metrics and simulation by-products with a review of the relevant literature to formulate the following recommendations for future sensor architectures:

- A large hour angle span benefits the *protect* mission by bringing more active geostationary spacecraft into view for change/manoeuvre detection, and also the *survey* mission by widening the 'fence' available to register objects on inclined orbits passing through the geostationary belt.
- Owing to the predominantly north-south motion of objects on inclined orbits, a large declination span serves to boost temporal coverage of registered objects.
- High-cadence observations can prevent trailing in acquired images, both for the targets of interest and background stars, boosting the signal-to-noise and improving the quality of the astrometric solution that feeds into orbital analysis.
- Surveillance regions with hour angle spans of around 1 hr and declination spans of less than 15° seem to offer the most cost-effective performance for the modalities considered, though it would be interesting to see how this varies with observational strategy.
- Ground-based optical imaging should be augmented by other sensing techniques to combat gaps in coverage due to daylight, poor weather conditions, and maintenance, for example infrared and/or event-based imaging.

We aim to conduct a follow-up study to build on these preliminary findings and investigate alternative observational strategies and sensing techniques.

ACKNOWLEDGEMENTS

JAB acknowledges support from the Defence Science and Technology Laboratory (Dstl, UK). The authors are grateful to Tim Flohrer and Vitali Braun from the Space Debris Office at the European Space Agency (ESA) for their sharing of the MASTER 8 reference population file.

REFERENCES

[1] J. A. Blake. Looking out for a sustainable space. *Astronomy & Geophysics*, 63(2):2–14, 2022.

[2] A. Lawrence, M. L. Rawls, M. Jah, A. Boley, F. Di Vruno, et al. The case for space environmentalism. *Nature Astronomy*, 6(4):428–435, 2022.

[3] HM Government. National Space Strategy, UK. https://www.gov.uk/government/publications/national-space-strategy. Accessed: 2023-08-08.

[4] J. A. Blake, K. Courtney, R. Dinsley, S. Eves, et al. The Global Network On Sustainability In Space (GNOSIS): Activities, Initiatives, and Future Endeavours. In *Proceedings of the Advanced Maui Optical and Space Surveillance (AMOS) Technologies Conference*, 2022.

[5] UKSA, CGI, GNOSIS, and UKspace. UKSA Space Domain Awareness Study. https://www.ukspace.org/wp-content/uploads/2022/07/UKSA-SDA-Study-Report_v2.4.pdf. Accessed: 2023-08-08.

[6] S. George, A. Agathanggelou, G. Privett, P. Halpin, et al. Phantom Echoes 2: A Five-Eyes SDA Experiment on GEO Proximity Operations. In *Proceedings of the Advanced Maui Optical and Space Surveillance (AMOS) Technologies Conference*, 2021.

[7] B. Weeden and V. Samson. *Global counterspace capabilities: an open source assessment*. Secure World Foundation Washington, DC, 2023.

[8] J. A. Blake, P. Chote, D. Pollacco, W. Feline, et al. DebrisWatch I: A survey of faint geosynchronous debris. *Advances in Space Research*, 67(1):360–370, 2021. doi: https://doi.org/10.1016/j.asr.2020.08.008.

[9] J. A. Blake, P. Chote, and D. Pollacco. Optical imaging of faint geosynchronous debris with the Isaac Newton Telescope. In *Proceedings of the Advanced Maui Optical and Space Surveillance (AMOS) Technologies Conference*, 2019.

[10] T. Schildknecht, A. Vananti, E. Cordelli, and T. Flohrer. ESA optical surveys to characterize recent fragmentation events in GEO and HEO. *Proceedings of the Advanced Maui Optical and Space Surveillance (AMOS) Technologies Conference*, page 34, 2019.

[11] P. M. Cunio, M. Bantel, B. R. Flewelling, W. Therien, et al. Photometric and Other Analyses of Energetic Events Related to 2017 GEO RSO Anomalies. In *Proceedings of the Advanced Maui Optical and Space Surveillance (AMOS) Technologies Conference*, 2017.

[12] Space-Track API. https://www.space-track.org/. Accessed: 2023-08-31.

[13] P. Chote, J. A. Blake, and D. Pollacco. Precision Optical Light Curves of LEO and GEO Objects. In *Proceedings of the Advanced Maui Optical and Space Surveillance (AMOS) Technologies Conference*, Precision Optical Light Curves of LEO and GEO Objects, 2019.

[14] V. Braun, A. Horstmann, S. Lemmens, C. Wiedemann, et al. Recent developments in space debris environment modelling, verification and validation with MASTER. In *Proceedings of the 8th European Conference on Space Debris*, page 18. ESA Space Debris Office Darmstadt, Germany, 2021.

[15] ESA. Space Debris Office: ESA's Annual Space Environment Report. GEN-DB-LOG-00288-OPS-SD, 2023.

[16] T. P. Robitaille, E. J. Tollerud, P. Greenfield, M. Droettboom, et al. Astropy: A community Python package for astronomy. *Astronomy & Astrophysics*, 558:A33, 2013.

[17] A. M. Price-Whelan, B. M. Sipőcz, H. M. Günther, P. L. Lim, et al. The Astropy project: Building an open-science project and status of the v2. 0 core package. *The Astronomical Journal*, 156(3):123, 2018.

[18] John D Hunter. Matplotlib: A 2d graphics environment. *Computing in science & engineering*, 9(03):90–95, 2007.

[19] Charles R Harris, K Jarrod Millman, Stéfan J Van Der Walt, Ralf Gommers, Pauli Virtanen, David Cournapeau, Eric Wieser, Julian Taylor, Sebastian Berg, Nathaniel J Smith, et al. Array programming with numpy. *Nature*, 585(7825):357–362, 2020.

[20] J. A. Blake. Software (open source): tlemcee. https://github.com/jblake95/tlemcee. Accessed: 2023-08-11.

[21] B. Rhodes. Skyfield: High precision research-grade positions for planets and Earth satellites generator. *Astrophysics Source Code Library*, pages ascl–1907, 2019.

[22] D. Vallado, P. Crawford, R. Hujsak, and T. S. Kelso. Revisiting spacetrack report# 3. In *AIAA/AAS Astrodynamics Specialist Conference and Exhibit*, page 6753, 2006.

[23] D. A. Vallado and P. J. Cefola. Two-line element sets–practice and use. In *63rd International Astronautical Congress, Naples, Italy*, pages 1–14, 2012.

[24] T. Schildknecht. Optical surveys for space debris. *The Astronomy and Astrophysics Review*, 14(1):41–111, 2007.

[25] J. A. Blake. *Optical imaging of space debris in low and high altitude orbits*. PhD Thesis: University of Warwick, 2021. URL `https://doi.org/10.13140/RG.2.2.11557.22247`.

[26] G. A. McCue, J. G. Williams, and J. M. Morford. Optical characteristics of artificial satellites. *Planetary and Space Science*, 19(8):851–868, 1971.

[27] D. S. McKnight and F. R. Di Pentino. New insights on the orbital debris collision hazard at GEO. *Acta Astronautica*, 85:73–82, 2013.

[28] P. V. Anderson, D. S. McKnight, F. D. Pentino, and H. Schaub. Operational considerations of GEO debris synchronization dynamics. In *66th International Astronautical Congress, IAC-15 A*, volume 6, page 7, 2015.

[29] J. A. Blake, P. Chote, D. Pollacco, D. Veras, A. Ash, et al. Supplementing a survey of geosynchronous debris with commercial-off-the-shelf equipment. In *Proceedings of the Advanced Maui Optical and Space Surveillance (AMOS) Technologies Conference*, 2020.

[30] E. Kerr, G. P. Elisabeth, P. Talon, D. Petit, et al. Using ai to analyse light curves for geo object characterisation. In *Proceedings of the Advanced Maui Optical and Space Surveillance (AMOS) Technologies Conference*, 2021.

[31] B. F. Cooke, P. Chote, D. Pollacco, R. West, et al. Simulated recovery of LEO objects using sCMOS blind stacking. *Advances in Space Research*, 2023.

[32] A. Milani, G. F. Gronchi, M. D. M. Vitturi, and Z. Knežević. Orbit determination with very short arcs. I admissible regions. *Celestial Mechanics and Dynamical Astronomy*, 90:57–85, 2004.

[33] J. L. Worthy III and M. J. Holzinger. Incorporating uncertainty in admissible regions for uncorrelated detections. *Journal of Guidance, Control, and Dynamics*, 38(9):1673–1689, 2015.

[34] K. Fujimoto and K. T. Alfriend. Optical short-arc association hypothesis gating via angle-rate information. *Journal of guidance, Control, and Dynamics*, 38(9):1602–1613, 2015.

[35] L. Pirovano, D. A. Santeramo, R. Armellin, P. Di Lizia, et al. Probabilistic data association: the orbit set. *Celestial Mechanics and Dynamical Astronomy*, 132(2):1–27, 2020.

[36] P. M. Cunio and B. Kirkpatrick. Assessment of Real-World Incident Types and Rates in Geosynchronous Orbit. In *Proceedings of the 8th Space Traffic Management Conference*, 2022.

[37] J. M. Krezan, S. Howard, P. D. Dao, and D. Surka. GEO collisional risk assessment based on analysis of NASA-WISE data and modeling. In *Proceedings of the Advanced Maui Optical and Space Surveillance (AMOS) Technologies Conference*, 2015.

[38] H. Krag, H. Klinkrad, R. Jehn, S. Flegel, et al. Conclusions from ESA Space Debris Telescope Observations on Space Debris Environment Modelling. In *Proceedings of the European Conference on Space Debris, Darmstadt, Germany*, 2009.

[39] P. Seitzer, S. M. Lederer, E. S. Barker, H. Cowardin, et al. A search for optically faint GEO debris. In *Proceedings of the Advanced Maui Optical and Space Surveillance (AMOS) Technologies Conference*, pages 13–16, 2011.

[40] D. L. Oltrogge, S. Alfano, C. Law, A. Cacioni, et al. A comprehensive assessment of collision likelihood in Geosynchronous Earth Orbit. *Acta Astronautica*, 147:316–345, 2018.

[41] Gunter's Space Page "Ascent". https://space.skyrocket.de/doc_sdat/ascent.htm. Accessed: 2023-08-31.

[42] M. Pyrak and J. Anderson. Performance of Northrop Grumman's Mission Extension Vehicle (MEV) RPO Imagers at GEO. In *Proceedings of the Advanced Maui Optical and Space Surveillance (AMOS) Technologies Conference*, 2021.

[43] S. M. Lederer, C. L. Cruz, B. A. Buckalew, P. Hickson, et al. NASA's Orbital Debris Optical Program: ESMCAT Nearing Full Operational Capability (FOC). In *Proceedings of the Advanced Maui Optical and Space Surveillance (AMOS) Technologies Conference*, 2020.

[44] J. Shaddix, J. Brannum, A. Ferris, A. Hariri, et al. Daytime GEO Tracking with" Aquila": Approach and Results from a New Ground-Based SWIR Small Telescope System. In *Proceedings of the Advanced Maui Optical and Space Surveillance (AMOS) Technologies Conference*, page 82, 2019.

[45] T. Kelecy, E. Gerber, S. Akram, and J. Paffett. Characterization of Resident Space object States Using Functional Data Analysis. *The Journal of the Astronautical Sciences*, 69(2):627–649, 2022.

[46] A. Bloom, J. Wysack, J. D. Griesbach, and A. Lawitzke. Space and Ground-Based SDA Sensor Performance Comparisons. In *Proceedings of the Advanced Maui Optical and Space Surveillance (AMOS) Technologies Conference*, 2022.

[47] J. Davis, T. Jennings-Bramly, J. Symons, and F. Waltho. Sensor Management for Space-Based Sensing Constellations. In *Proceedings of the Advanced Maui Optical and Space Surveillance (AMOS) Technologies Conference*, 2022.

[48] G. Cohen, S. Afshar, B. Morreale, T. Bessell, et al. Event-based sensing for space situational awareness. *The Journal of the Astronautical Sciences*, 66:125–141, 2019.

[49] A. Jolley, S. Afshar, G. Cohen, R. Lazarus Pahlavani, et al. Neuromorphic Sensor Event-Rate Monitoring for Satellite Characterization. *Journal of Spacecraft and Rockets*, 60(3):753–764, 2023.